Acta of Bioengineering and Biomechanics
Vol. 18, No. 2, 2016

Original paper
DOI: 10.5277/ABB-00373-2015-03

Patient-specific hemodynamics and stress-strain state of cerebral aneurysms

DMITRY IVANOV*, ALEKSANDR DOL, ASEL POLIENKO

Saratov State University, Educational-Research Institute of Nanostructures and Biosystems, Saratov, Russia.

Purpose: Approximately 5% of the adult population has one or more cerebral aneurysm. Aneurysms are one of the most dangerous cerebral vascular pathologies. Aneurysm rupture leads to a subarachnoid hemorrhage with a very high mortality rate of 45–50%. Despite the high importance of this disease there are no criteria for assessing the probability of aneurysm rupture. Moreover, mechanisms of aneurysm development and rupture are not fully understood until now. *Methods*: Biomechanical and numerical computer simulations allow us to estimate the behavior of vessels in normal state and under pathological conditions as well as to make a prediction of their postoperative state. Biomechanical studies may help clinicians to find and investigate mechanical factors which are responsible for the initiation, growth and rupture of the cerebral aneurysms. *Results*: In this work, biomechanical and numerical modeling of healthy and pathological cerebral arteries was conducted. Patient-specific models of the basilar and posterior cerebral arteries and patient-specific boundary conditions at the inlet were used in numerical simulations. A comparative analysis of the three vascular wall models (rigid, perfectly elastic, hyperelastic) was performed. Blood flow and stress-strain state of the two posterior cerebral artery aneurysm models was compared. *Conclusions*: Numerical simulations revealed that hyperelastic material most adequately and realistically describes the behavior of the cerebral vascular walls. The size and shape of the aneurysm have a significant impact on the blood flow through the affected vessel and on the effective stress distribution in the aneurysm dome. It was shown that large aneurysm is more likely to rupture than small aneurysm.

Key words: *hyperelastic material, numerical simulation, effective stress, blood flow, cerebral aneurysm*

1. Introduction

One of the cases of subarachnoid hemorrhage is an aneurysm rupture. Cerebral aneurysms are pathological dilatations of the Willis circle arteries. While only 2–5% of the world population [6], [3] are affected, aneurysm rupture leads to subarachnoid hemorrhage with a very high rate of mortality (40–50%) [2], [17].

Many researches showed that mechanical factors (hemodynamic forces, blood pressure, wall shear stress) play main role in processes of aneurysm initiation, growth and rupture [24], [4], [16]. Aneurysms are mainly formed in the apex of artery bifurcations due to high hemodynamic stresses in this region. Moreover, it was shown that wall shear stress (WSS) defines the initial growth of the aneurysm due to its influence on the endothelium [13]. Aneurysm growth is associated with low blood velocity in the dome. Rupture usually occurs in the dome. However, it remains unclear what geometrical and/or mechanical factor plays the main role and determine the rupture. The most studied mechanical factor is WSS [15]. Moreover, modern medical diagnostic methods are not able to answer the question on the probability of the aneurysm future behavior and/or rupture.

Today the decision for treating cerebral aneurysms is based on patients history, aneurysm size and location. The critical size is the most discussed parameter. Now there is a need for more dependable and precise factor or criteria for assessing the risk of aneurysm rupture for each patient based on patient-specific blood flow simulation.

* Corresponding author: Dmitry Ivanov, Saratov State University, Educational-Research Institute of Nanostructures and Biosystems, 83 Astrakhansaya street, 410012 Saratov, Russia. Tel: +79173146807, e-mail: ivanovdv@gmail.com

Received: May 5th, 2015
Accepted for publication: July 6th, 2015

Computational fluid dynamics and, in particular, fluid-structure interaction simulations, are the only method of predicting surgical operations and behavior of the cerebral arteries [19], [22], [10], [23]. However, in such simulations, it is important to consider not only the patient-specific geometry but also patient-specific arterial mechanical characteristics, individualized boundary conditions for the blood flow at inlets and outlets.

This paper presents results of the patient-specific numerical modeling of the cerebral arteries behavior in normal state and with two different aneurysm models. A comparative analysis of the three wall models (rigid, perfectly elastic and hyperelastic) was conducted. A study of the blood flow through the basilar artery and posterior cerebral arteries (PCA) with two aneurysm models of the left PCA was performed with the help of finite element method.

The main aim of this study was to provide new information to clinicians for better understanding of the processes of the aneurysm initiation, growth and rupture.

2. Material and methods

3D models of the arteries and aneurysm were built on the basis of the contrast Magnetic Resonance Imaging (MRI). Figure 1 shows all the 3D models which were used in numerical simulations. Technique for creating 3D models is described in detail in our previous work [7]. Vascular wall was built on the basis of morphological data provided by anatomy department of Saratov State Medical University which is also described in [7].

Final 3D models were exported into Ansys Workbench 15.0 (Ansys Inc., Canonsburg, PA, USA) as Parasolid format (x_t) for tetrahedral meshing and numerical simulation. We used inflation method for the flow domain mesh creation. This method allowed us to create boundary layers of prism elements. Such layers are critical for accuracy and capturing the near wall flow physics while conducting computational fluid dynamics calculations. The number of inflation layers, as well as the characteristic size of a mesh, was calculated on the basis of the mesh independence analysis with the help of the mesh refinement tests. The total number of solid elements was about 11500. Total number of fluid elements was about 70000 for each model.

Patient-specific boundary conditions for carotid and vertebral arteries were obtained on the basis of ultrasound data [7]. The velocity profile assumed to be rectangular. In [18], the authors showed that rectangular velocity profile does not affect the blood flow in the aneurysm. Moreover, in numerical calculations we used 3D models with long sections of the basilar artery to minimize influence of the rectangular velocity profile on the blood flow in aneurysms.

Blood was assumed as incompressible, homogeneous and Newtonian fluid with constant density of 1050 kg/m^3 and dynamic viscosity of 0.0037 Pa·s. In [11], it was shown that non-Newtonian characteris-

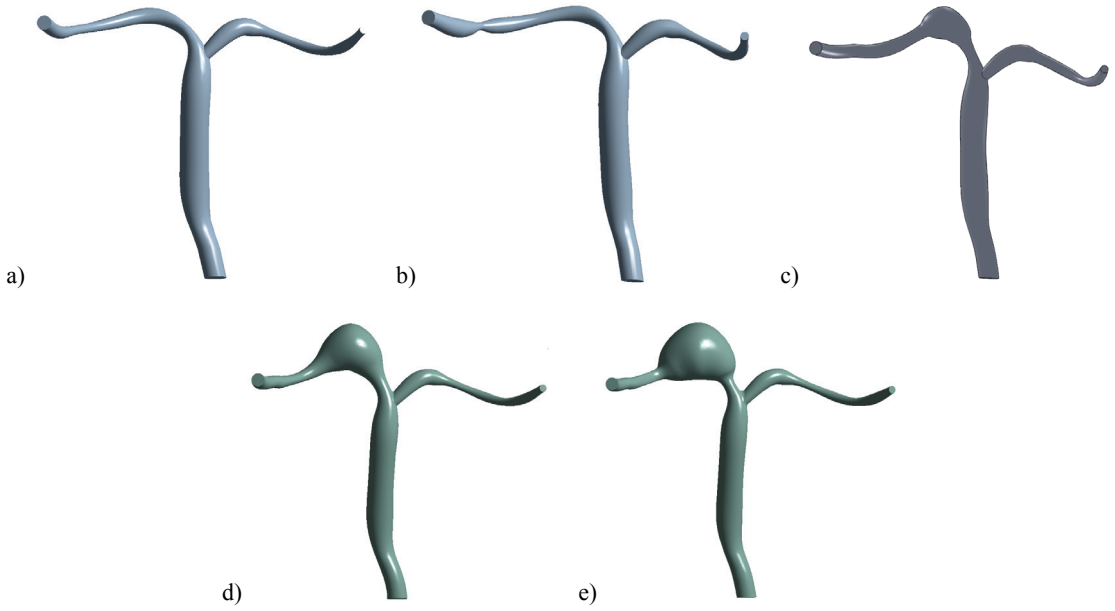

Fig. 1. Basilar artery with PCA: (a) normal state, (b) with 40% stenosis, (c) aneurysm (5.5 mm length, 3.5 mm height), (d) aneurysm (7.5 mm length, 5 mm height), (e) aneurysm (10 mm length, 7.5 mm height)

tics of the blood should be considered only in vessels with a small diameter (about and less than 0.1 mm) where the shear rates are very small. Blood flow was governed by Navier–Stokes equations for a moving domain.

Three types of vessel walls were investigated: rigid, perfectly elastic with Young's modulus of 5 MPa [24] and Poison's ratio of 0.49 and hyperelastic Mooney–Rivlin model [7] and density of 1400 kg/m^3. The Mooney–Rivlin strain energy function used in this research is presented in the following equation

$$W = C_1(I_1 - 3) + C_2(I_2 - 3) + C_3(I_1 - 3)(I_2 - 3) \quad (1)$$

where W – strain energy function of the material, I_1, I_2 – the Cauchy–Green strain tensor invariants, C_1, C_2, C_3 – material parameters which were calculated from the mechanical experiments.

Comparative analysis for these three wall models was performed for normal artery, artery with stenosis and with aneurysm (Fig. 1a–c).

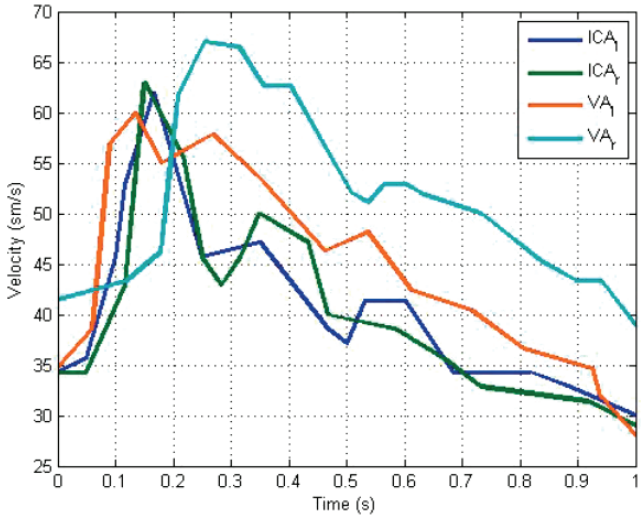

Fig. 2. Blood flow in carotid and vertebral arteries

The boundary conditions for the inlet velocity are presented in Fig. 2. We stated zero pressure condition for blood [5] at the outlets. No-slip boundary conditions were applied at the blood–wall interface. Inlet and outlet vessel ends were fixed.

Numerical calculations were performed in Ansys Workbench. FSI problems were solved. We used two modules for the calculations – Ansys CFX for blood flow and Ansys Structural – for the vessel wall stress-strain state calculation. This approach assumes that hemodynamic forces are calculated and transferred to the vessel wall in each time step. Then at the same time step vessel wall stress-strain state is calculated and deformations are transferred to the blood flow. Thus, in the next time step blood flow is calculated in new boundaries due to the displacements and deformations of the vessel wall. Each model was simulated for two cardiac cycles during 2 seconds. Coupled time step of 0.005 s was used. Numerical results from the second cycle were analyzed in Ansys CFD-Post.

3. Results

Comparative analysis of the three arterial wall models

Three models of the basilar artery-PCA bifurcation were investigated. We assumed left PCA in normal state, in the case of 40% stenosis and with aneurysm. Blood flows through the left PCA were compared for the three vessel wall models: rigid, perfectly elastic and hyperelastic. Blood flows at the left PCA outlet in the case of rigid vessel walls are shown in Fig. 3. Curves in Fig. 3 show that the blood flow for healthy left PCA and left PCA with aneurysm do not differ during cardiac cycle. Blood flow for left PCA with stenosis is decreased by 10% on average.

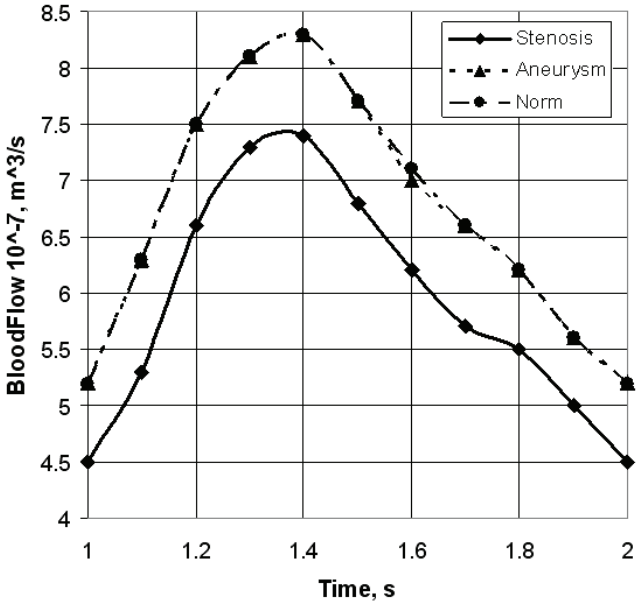

Fig. 3. Blood flow in left PCA in the case of rigid walls

A similar situation was observed for the case of perfectly elastic walls, which is shown in Fig. 4.

The situation with blood flows changed when hyperelastic model was considered. Left PCA in

normal state showed the highest blood flow (solid line in Fig. 5). Blood flow through the left PCA with aneurysm decreased by 6% compared with healthy artery. Blood flow through the stenosed left PCA was decreased by 11% compared with healthy artery.

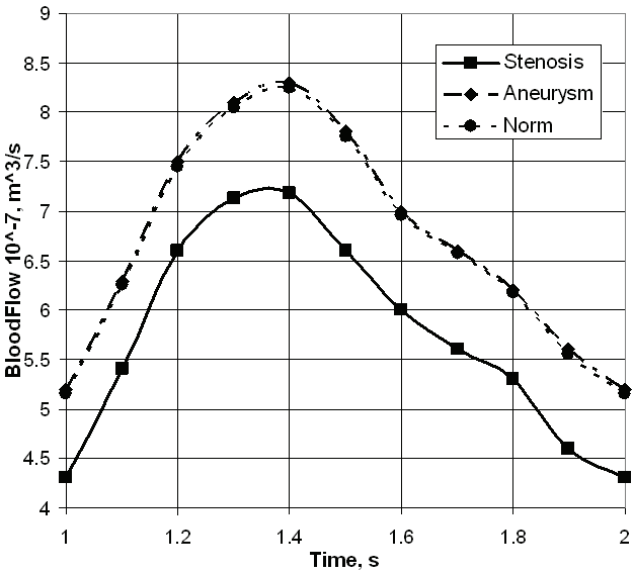

Fig. 4. Blood flow in left PCA
in the case of perfectly elastic walls

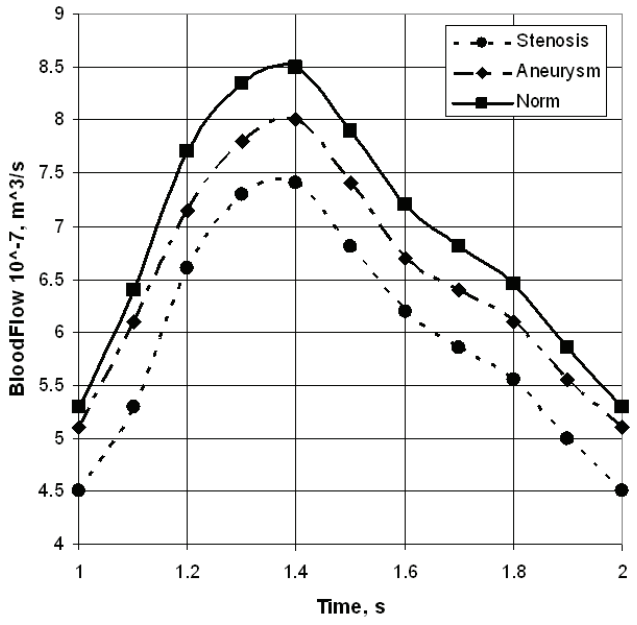

Fig. 5. Blood flow in left PCA in the case of hyperelastic walls

So, the Mooney–Rivlin hyperelastic model with three constants was used in further calculations. This model showed the most adequate and realistic results in a comparative analysis conducted for the healthy, stenosed left PCA and artery with aneurysm.

Models of the basilar artery-PCA aneurysms

Two models of the left PCA with small and large aneurysms were investigated. Aneurysm models and their sizes are shown in Fig. 1d, e.

Blood flows at the outlets of the left PCA for both models are shown in Fig. 6. It can be seen that increasing the size of the aneurysm entails reducing the blood flow at the outlet of the affected artery. The difference in blood flow rates for the two models considered was about 17%.

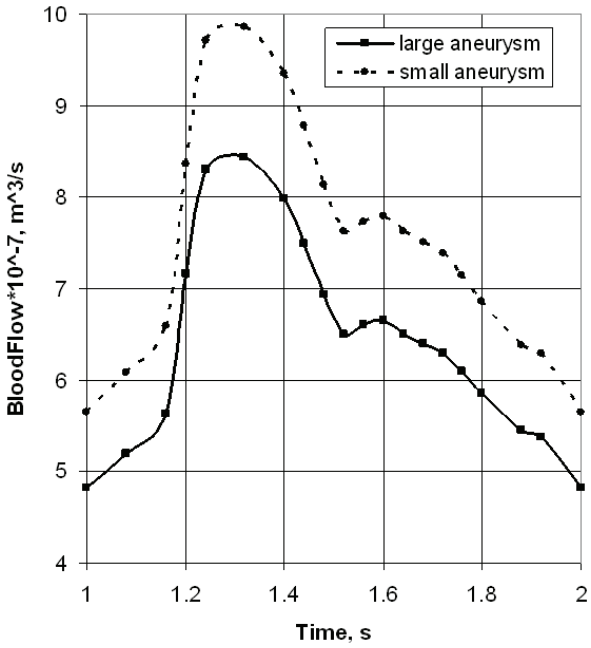

Fig. 6. Blood flow in left PCA for large and small aneurysms

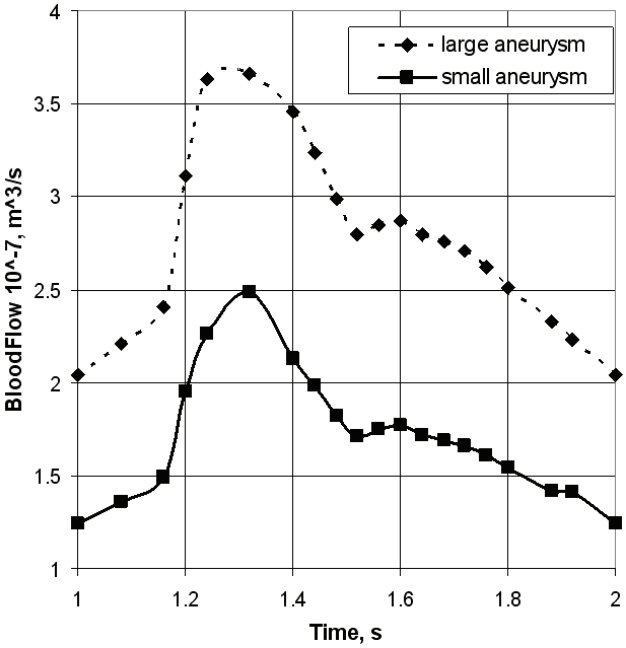

Fig. 7. Blood flow in right (healthy) PCA
for large and small aneurysms

Blood flows at the outlets of the right healthy PCA for both aneurysm models are shown in Fig. 7. The graphs show that the decrease in blood flow through the pathological left PCA (solid line in Fig. 6 corresponds to a larger aneurysm) in connection with the growth of the aneurysm leads to an increase of blood flow through the healthy branch (dashed line in Fig. 7 corresponds to a healthy right PCA for the larger aneurysm model).

WSS at systole for the two models are shown in Fig. 8a, b. The lowest WSS values (less than 1.5 Pa) are achieved in the dome of the aneurysms, where blood velocities are very small because of the blood swirling within the aneurysm (Fig. 8). WSS values were even lower at diastole due to reduced blood velocity at the inlet and reduced blood flow through the vessel.

Streamlines at systole for both aneurysm models are shown in Fig. 9. Streamlines show stagnation ar-

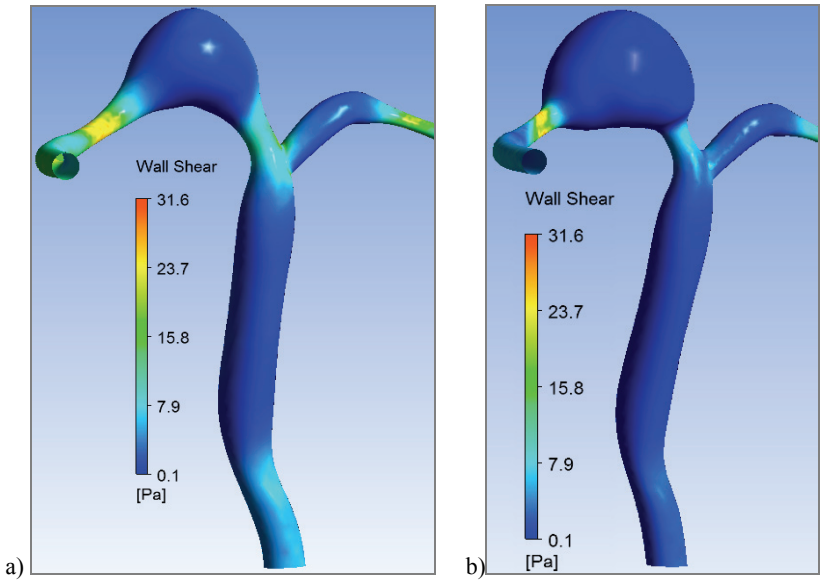

Fig. 8. WSS in systole for small (a) and large (b) aneurysm models

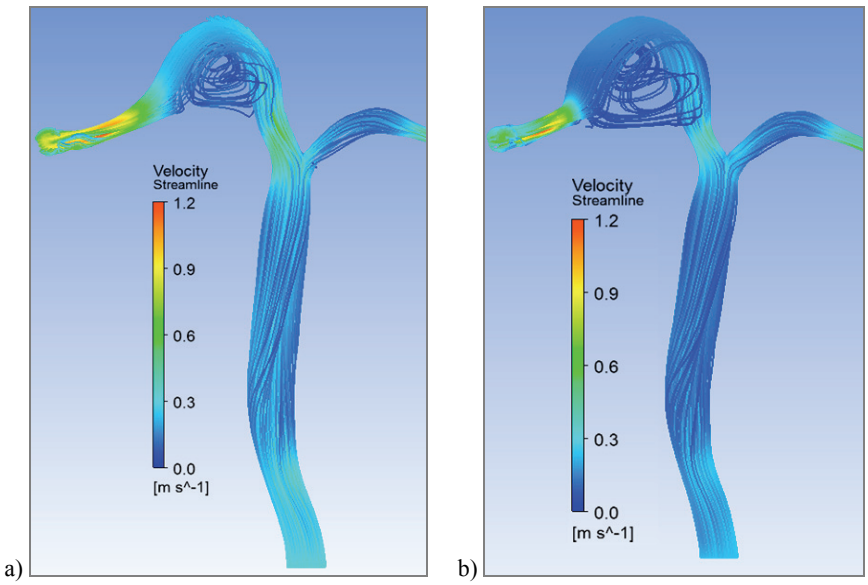

Fig. 9. Streamlines in systole for small (a) and large (b) aneurysm models

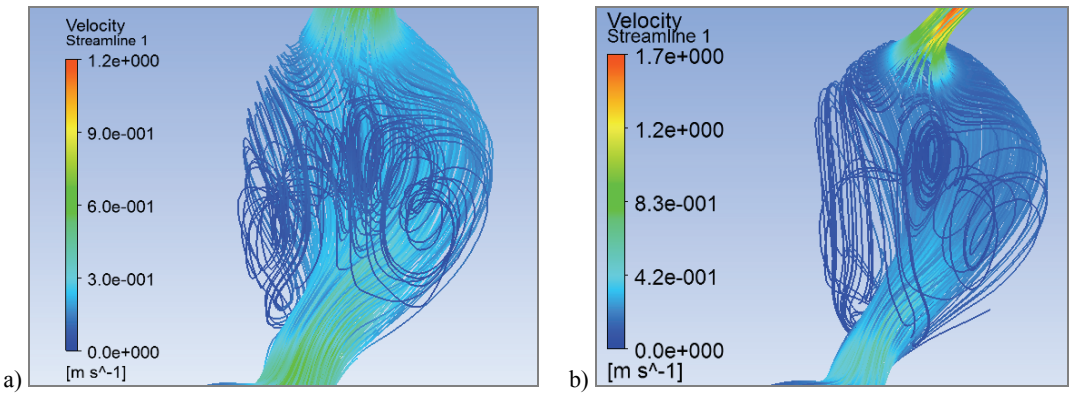

Fig. 10. Vortices in the aneurysm dome: (a) small aneurysm, (b) large aneurysm

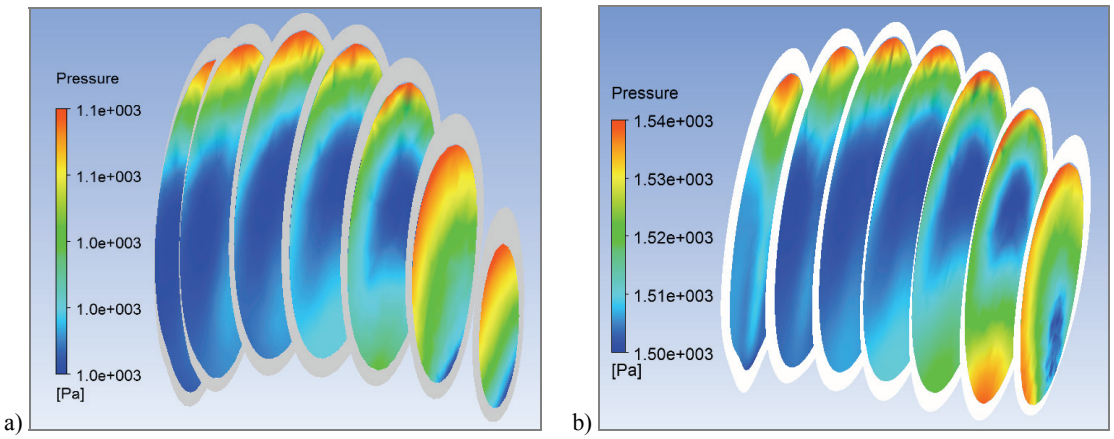

Fig. 11. Blood pressure fields in the aneurysm dome: (a) small ameurysm, (b) large aneurysm

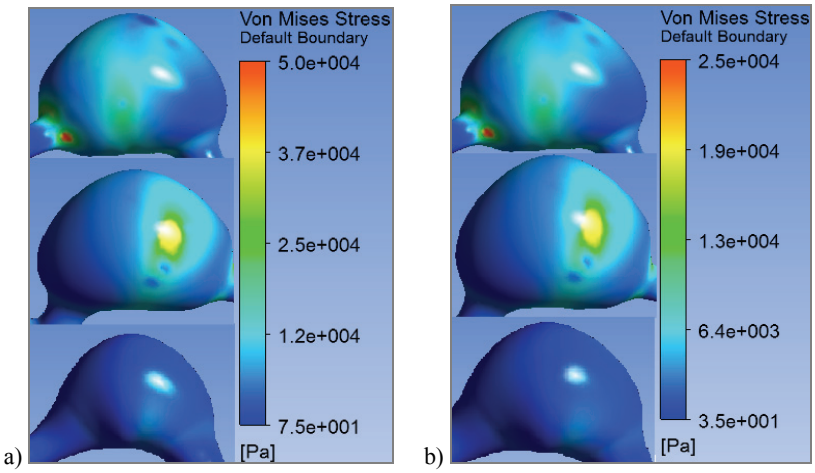

Fig. 12. Effective stresses in small and large aneurysm for systole (a) and diastole (b).
Large aneurysm – front view, Large aneurysm – back view, Small aneurysm – front view

eas with reverse flows in the aneurysm dome. The main blood flow passes aneurysm at the outer radius and extremely low blood velocities are concentrated at the bottom of the aneurysm dome.

Swirl in a small aneurysm is located symmetrically. Figure 10 clearly shows a single vortex, located across the dome of the aneurysm. Swirl in a larger aneurysm is located asymmetrically (Fig. 10b).

Blood pressure field for both aneurysms is uneven. The highest pressure values are concentrated at the upper part of the dome (Fig. 11a, b). The average pressure value was 1100 Pa for small and 1540 Pa for

large aneurysm. The difference in average pressure values for small and large aneurysms was about 33%. This shows that in the case of the same boundary conditions average pressure in large aneurysm was 33% higher than average pressure in small aneurysm.

Effective stresses (Fig. 12) in larger aneurysm were much higher than in small aneurysm. Effective stress field in small aneurysm was more uniform than in larger aneurysm. At the connection area of the large aneurysm and left PCA high stress concentrations were obtained which maintained their position during the entire cardiac cycle. Effective stress reaches 50 000 Pa in this region which is 3–4 times higher than maximum effective stress value in the small aneurysm.

4. Discussion

In this article, we presented results of the patient-specific cerebral aneurysms fluid-structure simulations. We have numerically investigated basilar arteries and PCA in normal state, with stenosis and aneurysms of different sizes.

The first part of the present research was dedicated to the vessel wall model selection. We compared 3 types of the wall models: rigid, perfectly elastic and hyperelastic. Next, we considered two patient-specific aneurysms of the left PCA taking into account patient-specific boundary conditions at the inlet. Length of the large aneurysm was greater than the length of the small aneurysm by 33%. Height of the large aneurysm was greater than the height of the small aneurysm by 50%. We analyzed blood flows at the outlets of the pathological and healthy PCA. Pressures in aneurysm sac, streamlines, WSS and effective stress fields were analyzed for both models.

The conclusions of this study are important not only from a computational point of view, but also from the biomechanics point of view, as they contribute to the discussion on the mechanical factors influence on the formation, growth and rupture of cerebral aneurysms.

The quality of the numerical calculations depends not only on the choice of method for solving boundary value problems, but also on competent formulation of the problem, the quality of the computational mesh, realistic geometric models and boundary conditions. In [18], a method (algorithm) for constructing smooth, realistic 3D models of vessels is presented. Authors employed the region growing method with intensity thresholding for image segmentation. This technique in contrast to our's [7] does not allow creating trifurcations. In this case, our method though is not automated, however, allows one to create realistic and smooth 3D models suitable for calculations and editing.

In [9], it was shown that the use of patient-specific boundary conditions at the inlet significantly changes the WSS distribution, vortices and flow in an aneurysm. So, in this research patient-specific models of the cerebral arteries with patient-specific boundary conditions at the inlet which were obtained with the help of ultrasound were investigated.

To account for the near-wall flow in the aneurysm and vessels tetrahedral mesh with 5 boundary prismatic layers was built (with decreasing thickness in the radial direction) by analogy to [20]. This important point about the mesh quality is not mentioned by many authors in their works.

On the basis of numerical results we concluded that hyperelastic model showed the most adequate and realistic behavior of the arterial wall. In [21], authors showed that linear model compared with hyperelastic overestimates shear stresses on the wall by 11%. This confirms our results that blood flow values in healthy artery and artery with aneurysm were the same for perfectly elastic walls. Nevertheless, in many recent papers [9], [8], authors still used rigid walls while modeling blood flow in aneurysm models. We are confident that such simplifications significantly affect hemodynamics of the healthy arteries and arteries with aneurysms.

We evaluated blood flows through the PCA for two different aneurysm models. It was found that the larger aneurysm significantly reduced blood flow downstream vessel. In this case, the blood flow in both branches of the PCA was stored and redistributed with a healthy PCA. Vortex in the dome of the small aneurysm during cardiac cycle remained symmetrical.

We have found significant heterogeneity of the effective stress distribution in the dome of the large aneurysm, which may indicate that it is more likely to rupture. Moreover, maximum value of the effective stress for the large aneurysm was twice as high as that for the small aneurysm. In [1], [19], authors obtained a higher effective stresses for ruptured aneurysms compared with unruptured aneurysms. It turns out that in this case the larger aneurysm is more prone to rupture than the small aneurysm. Higher average blood pressure value in large aneurysm may also indicate that it is more likely to rupture. Our results showed that average maximum pressure value in small aneurysm was 33% less than in large aneurysm with identical blood flow at the inlet of the basilar artery.

Certainly, there are a number of simplifications and limitations in this paper. First of all, the arterial wall is anisotropic and contains three layers. Homogeneous and isotropic wall model used in our computations may lead to inaccurate predictions of the wall deformation field and hemodynamic solution. It would be better to use healthy arterial tissue in parent vessels and collagenous tissue in the aneurysm part. Second, the wall thickness is practically impossible to obtain from tomograms. So, we used average morphological data for wall thickness parameter. For a more precise description of the stress-strain state of the wall and hemodynamics it is necessary to obtain morphological data for the wall thickness for each particular patient on the basis of medical diagnostic data. Also, instead of the zero boundary condition at the outlet more physiological boundary condition could be stated. We hope to pursue these problems in our future studies.

5. Conclusions

The results showed that hyperelastic wall model and interaction between blood and wall significantly alter hemodynamics of the aneurysm with respect to the rigid wall model. So, while modeling vascular wall behavior it is necessary to consider its nonlinear character. Patient-specific modeling needs both the geometry of the individual patient and the individual boundary conditions. Moreover, the geometry of an aneurysm is an important factor which determines hemodynamics and stress-strain state of the aneurysm wall.

Acknowledgements

The research was supported by Russian Foundation for Basic Research (project No. 12-01-31310 mol_a).

References

[1] BAZILEVS Y., HSU M.C., ZHANG Y., WANG W., KVAMSDAL T., HENTSCHEL S., ISAKSEN J.G., *Computational vascular fluid-structure interaction: methodology and application to cerebral aneurysms*, Biomech. Model Mechanobiol., 2010, Vol. 9(4), 481–498.

[2] BEDERSON J.B., CONNOLLY E.S., BATJER H.H., DACEY R.G., DION J.E., DIRINGER M.N., DULDNER J.E., HARBAUGH R.E., PATEL A.B., ROSENWASSER R.H., *Guidelines for the management of aneurysmal subarachnoid hemorrhage: a statement for healthcare professionals from a special writing group of the stroke council*, Stroke, 2009, Vol. 40(3), 994–1025.

[3] BONNEVILLE F., SOUROUR N., BIONDI A., *Intracranial aneurysms: an overview*, Neuroimaging Clin. N. Am., 2006, Vol. 16(3), 371–382.

[4] CASTRO M.A., PUTMAN C.M., CEBRAL J.R., *Patient-specific computational fluid dynamics modeling of anterior communicating artery aneurysms: a study of the sensitivity of intraaneurysmal flow patterns to flow conditions in thecarotidarteries*, Am. J. Neuroradiol., 2006, Vol. 27(10), 2061–2068.

[5] CEBRAL J.R., MUT F., RASCHI M., SCRIVANO E., CERATTO R., LYLYK P., PUTMAN C.M., *Aneurysm rupture following treatment with flow-diverting stents: computational hemodynamics analysis of treatment*, AJNR Am. J. Neuroradiol., 2011, Vol. 32(1), 27–33.

[6] CURTIS S.L., BRADLEY M., WILDE P., AW J., CHAKRABARTI S., HAMILTON M., MARTIN R., TURNER M., STUART A.G., *Results of screening for intracranial aneurysms in patients with coarctation of the aorta*, AJNR Am. J. Neuroradiol., 2012, Vol. 33(6), 1182–1186.

[7] IVANOV D., DOL A., PAVLOVA O., ARISTAMBEKOVA A., *Modeling of human circle of Willis with and without aneurisms*, Acta Bioeng. Biomech., 2014, Vol. 16(2), 121–129.

[8] JANIGA G., BERG P., SUGIYAMA S., KONO K., STEINMAN D.A., *The computational fluid dynamics rupture challenge 2013 – phase I: prediction of rupture status in intracranial aneurysms*, AJNR Am. J. Neuroradiol., 2015, Vol. 36(3), 530–536.

[9] JANSEN I.G., SCHNEIDERS J.J., POTTERS W.V., VAN OOIJ P., VAN DEN BERG R., VAN BAVEL E., MARQUERING H.A., MAJOIE C.B., *Generalized versus patient-specific inflow boundary conditions in computational fluid dynamics simulations of cerebral aneurysmal hemodynamics*, AJNR Am. J. Neuroradiol., 2014, Vol. 35(8), 1543–1548.

[10] KROON M., *Simulation of cerebral aneurysm growth and prediction of evolving rupture risk*, Modelling and Simulation in Engineering, 2011. DOI: 10.1155/2011/289523

[11] KU J.P., ELKINS C.J., TAYLOR C.A., *Comparison of CFD and MRI flow and velocities in an in vitro large artery bypass graft model*, Ann. Biomed. Eng., 2005, Vol. 33(3), 257–269.

[12] LEE C.J., ZHANG Y., TAKAO H., MURAYAMA Y., QIAN Y., *A fluid–structure interaction study using patient-specific ruptured and unruptured aneurysm: The effect of aneurysm morphology, hypertension and elasticity*, J. Biomech., 2013, Vol. 46(14), 2402–2410.

[13] LEHOUX S., TRONC F., TEDGUI A., *Mechanisms of blood flow-induced vascular enlargement*, Biorheology, 2002, Vol. 39(3–4), 319–324.

[14] MARZO A., SINGH P., REYMOND P., STERGIOPULOS N., PATEL U., HOSE R., *Influence of inlet boundary conditions on the local haemodynamics of intracranial aneurysms*, Computer Methods in Biomechanics and Biomedical Engineering, 2009, Vol. 12(4), 431–444.

[15] SADASIVAN C., FIORELLA D.J., WOO H.H., LIEBER B.B., *Physical factors effecting cerebral aneurysm pathophysiology*, Ann. Biomed. Eng., 2013, Vol. 41(7), 1347–1365.

[16] SHOJIMA M., OSHIMA M., TAKAGI K., TORII R., NAGATA K., SHIROUZU I., MORITA A., KIRINO T., *Role of the bloodstream impacting force and the local pressure elevation in the rupture of cerebral aneurysms*, Stroke, 2005, Vol. 36(9), 1933–1938.

[17] TEUNISSEN L.L., RINKEL G.J.E., ALGRA A., VAN GIJN J., *Risk factors for subarachnoid hemorrhage – a systematic review*, Stroke, 1996, Vol. 27(3), 544–549.

[18] TORII R., OSHIMA M., *An integrated geometric modelling framework for patient-specific computational haemodynamic study on wide-ranged vascular network*, Comput. Methods Biomech. Biomed. Engin., 2012, Vol. 15(6), 615–625.

[19] TORII R., OSHIMA M., KOBAYASHI T., TAKAGI K., TEZDUYAR T.E., *Fluid–structure interaction modeling of blood flow and cerebral aneurysm: significance of artery and aneurysm shapes*, Comput. Methods Appl. Mech. Eng., 2009, Vol. 198(45–46), 3613–3621.

[20] TURJMAN A.S., TURJMAN F., EDELMAN E.R., *Role of fluid dynamics and inflammation in intracranial aneurysm formation*, Circulation, 2014, Vol. 129(3), 373–382.

[21] VALENCIA A., BURDILES P., IGNAT M., MURA J., BRAVO E., RIVERA R., SORDO J., *Fluid structural analysis of human cerebral aneurysm using their own wall mechanical properties*, Comput. Math. Methods Med., 2013, 2013, 293128, DOI: 10.1155/2013/293128.

[22] VALENCIA A., LEDERMANN D., RIVERA R., BRAVO E., GALVEZ M., *Blood flow dynamics and fluid–structure interaction in patient-specific bifurcating cerebral aneurysms*, Int. J. Numer Method Biomed. Eng., 2008, Vol. 58(10), 1081–1100.

[23] WANG S., DING G., ZHANG Y., YANG X., *Computational haemodynamics in two idealised cerebral wide-necked aneurysms after stent placement*, Comput. Methods Biomech. Biomed. Engin., 2011, Vol. 14, 927–937.

[24] WANG X., LI X., *Biomechanical behaviour of cerebral aneurysm and its relation with the formation of intraluminal thrombus: a patient-specific modelling study*, Comput. Methods Biomech. Biomed. Engin., 2013, Vol. 16(11), 1127–1134, DOI: 10.1080/10255842.2011.